batteries

MDPI

Article

Tailoring Particle Size and Morphology to Enhance Performance and Safety of Glass-Based Battery Separators

Philipp Rank [1,2,*], Sebastian Müllner [3], Thorsten Gerdes [1,2] and Christina Roth [2,3]

[1] Keylab Glass Technology, Faculty of Engineering Science, University of Bayreuth, Prof.-Rüdiger-Bormann-Str. 1, 95447 Bayreuth, Germany; thorsten.gerdes@uni-bayreuth.de
[2] Bavarian Center for Battery Technology (BayBatt), Universitätsstraße 30, 95447 Bayreuth, Germany; christina.roth@uni-bayreuth.de
[3] Electrochemical Process Engineering, Faculty of Engineering Science, University of Bayreuth, Universitätsstraße 30, 95447 Bayreuth, Germany
* Correspondence: philipp.rank@uni-bayreuth.de

Abstract

The thermal characteristics and surface properties of battery separators are commonly modified by the incorporation of inorganic particles into a polymeric matrix material. At present, the particles employed are predominantly of an arbitrary shape. Herein, we demonstrate significantly improved battery safety features using a glass-based separator consisting of platelet-shaped particles. Glass is selected due to its temperature stability and the freedom of design that it offers when particles are formed directly from the melt. The influence of the particles' aspect ratio and layer stacking on the electrochemical properties was analyzed, and a parametric study of glass particle layers as function of edge length and thickness was conducted. Particles with an excessively high aspect ratio impede the Li^+ diffusion pathway, thereby negatively affecting the performance and stability of the battery cell. Conversely, if the aspect ratio is insufficient, a deterioration in cell performance can be observed, particularly at elevated C-rates, due to the high specific surface area of the particles. Hence, the utilization of particles with a moderate aspect ratio of about 10 and a thickness of around 1 µm is proposed to ensure optimum performance.

Keywords: lithium-ion batteries; separator; Si anode; glass particles; safety features

Academic Editor: Yong-Joon Park

Received: 25 September 2025
Revised: 17 October 2025
Accepted: 20 October 2025
Published: 22 October 2025

Citation: Rank, P.; Müllner, S.; Gerdes, T.; Roth, C. Tailoring Particle Size and Morphology to Enhance Performance and Safety of Glass-Based Battery Separators. *Batteries* **2025**, *11*, 388. https://doi.org/10.3390/batteries11110388

1. Introduction

With advantages such as high energy density, low self-discharge and light weight, thus resulting in high specific energy and power, lithium-ion batteries (LIBs) dominate the major energy storage markets, particularly for mobile devices and electric vehicles. One of the key components in liquid electrolyte batteries is the separator, as it ensures safe transport, handling and operation of the battery. Its function is to physically and electronically separate the two electrodes while allowing for unhindered ionic transport. The basic requirements for a separator include chemical and electrochemical stability with respect to the electrolyte and the potential window of the electrodes. Furthermore, high open porosity is required to enable absorption and retention of the electrolyte [1]. In addition, the separator must be robust enough to withstand the mechanical stress of the cell assembly. According to the state of the art, a separator should be as thin and lightweight as possible in order not to affect the specific (gravimetric and volumetric) energy density of the battery [2]. On the other hand, the separator represents the safety-relevant component of the cell and must be able to prevent the formation and growth of dendrites during the charging/discharging process [3]. A recent

publication by Seo et al. on mechanical shutdown of battery separators ultimately leading to silicon anode failure further underscores the necessity to improve separator materials, in particular for future-oriented technologies utilizing lithium (Li) metal or silicon anodes [4]. These materials are known to undergo significant volumetric change during cycling, which can compromise the structural integrity and safety of the battery.

Lithium metal batteries (LMBs) are considered a promising candidate for the next generation of batteries as they offer excellent advantages in terms of high theoretical specific capacity (3860 mAh g^{-1}) and the lowest redox potential (−3.04 V versus the standard hydrogen electrode) [5]. This is of particular relevance for emerging high-energy applications, for instance, in long-range and heavy-duty electric vehicles, as the highest energy density that conventional LIBs can deliver is far from the demands of these fields. However, the practical application of lithium metal in secondary batteries is limited by the growth of Li dendrites, which is of particular significance for lithium–metal and lithium–sulfur batteries [6,7]. Additionally, in fast-charging applications under harsh conditions, lithium plating is observed on the anode side [8]. If only a single dendrite resulting from accidental or inhomogeneous deposition of metallic lithium (i.e., Li plating) penetrates the separator and forms a conductive path between the two electrodes, a short circuit in the battery will lead to its immediate and fatal failure [3,9].

Since battery safety is of paramount importance, the separator is playing a crucial role in the introduction of lithium metal batteries to the market [10]. Fast market penetration of such technologies is therefore strongly dependent on new developments targeted towards tailored, functional and smart separator materials. The enormous increase in energy density compared to current anode materials such as graphite also opens up new design space for separators that enable the safe operation of these batteries [10]. During cell operation, the micro-roughness of Li electrode surfaces causes an inhomogeneous distribution of Li ions, followed by the formation of Li dendrites [11]. Instead of modifying the lithium surface to allow for more homogeneous plating [12–14], a more practical approach would be the modification of the separator with functional and thermally stable particles [11,15,16]. Even when accounting for the additional mass resulting from the separator engineering through the incorporation of particles, the specific energy density will still exceed that of conventional LIBs to a significant extent.

A variety of materials have been suggested as suitable particles in separators, the majority of which are alumina or boehmite [2,3,17–22]. While the thermal stability of these inorganic materials is superior in comparison to that of polymers, their density is higher due to their crystalline nature. Despite the inherent rigidity of glass materials, previous studies also demonstrated the successful application of glass-based separators in LIBs [23,24]. Glasses offer an optimum compromise between low density and high temperature stability, thereby ensuring safe operation even at higher (dis-)charging rates or in the event of internal damage or external abuse [25]. Amorphous silicate glasses, in particular, offer a broad stability window with maximum service temperatures of at least 600 °C, which is sufficient for battery applications. Another advantage of glass as separator material is its capability to be processed directly from the melt into particles [24,26]. This allows a high degree of freedom in the choice and control of particle morphology and size.

Yuan et al., for instance, proposed that the incorporation of heterogeneous particles within the separator can mitigate and suppress dendrite growth-induced internal short-circuits in solid-state batteries [27]. In their study, the aspect ratio of the embedded particles, together with their alignment in layered structures, was found to dominate the dendrite mitigation effect. Specifically, multiple particles with a medium aspect ratio, arranged in a brick-and-mortar-like configuration, were shown to fully mitigate dendrite penetration. In contrast, particles with a small aspect ratio merely extended the dendrite growth path,

resulting in a delayed but not prevented short-circuit. These results reveal that adding heterogeneous blocks with high fracture resistance is a promising approach to mitigate dendrites and reduce the risk of short-circuits in batteries [27]. Also, Rafiz et al. successfully used boehmite plates to suppress lithium dendrite growth by increasing the tortuosity of their separators [15].

The practical implementation of the above findings, however, requires additional consideration of the actual microstructural effects, like orientation and packing density of the particles. For liquid electrolyte systems, this is particularly important with regard to the influence of particles on the ionic conductivity of the system, especially when using non-conductive inorganic particles. In this case, the porosity and tortuosity of the particle-filled or -coated separator are essential. Schadeck et al. already explored the general suitability of platelet-shaped glass particles for separator applications [23,24]. However, the size and morphology of the utilized particles also have a significant impact on the manufacturing process. They will affect slurry processability and separator formation, and consequently the final electrochemical performance. Although studies that investigated the influence of separator particles of varying sizes, both spherical and arbitrarily shaped, on the electrochemical performance can already be found in the literature [28–34], there are only a few references for the impact of particle shape [30,35]. Notably, none of these references include variations in platelet-shaped particles.

We herein propose adding platelet-shaped particles in a controlled fashion to separators for lithium battery systems, inspired by the "brick-and-mortar" toughening mechanism [27]. In particular, we evaluate the fundamental influence of the morphology of platelet-shaped glass particles on the physico- and electrochemical properties of the system, focusing on the challenges of volume-modulating anode materials like lithium and silicon. For the first time, a quantitative parametric study of glass particle layers as a function of the edge length and the thickness is carried out in order to significantly enhance the safety features of battery separators comprising these.

2. Materials and Methods

2.1. Materials

The rotary atomization of a glass melt results in a wide range of particle morphologies that can be categorized by shape and structure. A detailed description of the processing route can be found in the publications of Kyrgyzbaev et al. [36] and Schadeck et al. [24]. The platelet-shaped particles (glass flakes) produced by this process vary considerably in thickness D and edge length L. Due to the manufacturing process of glass flakes by rotary atomization, their thickness is defined by processing parameters such as viscosity, temperature and rotational speed. The edge length is adjusted by subsequent milling and classifying [24,26,36].

In this study, commercially available glass flakes (Glassflake Ltd., Leeds, UK) of various sizes in terms of thickness and edge length, according to the manufacturer's data sheet (see Table S1 in Supplementary Materials), were analyzed to determine their suitability for incorporation into separator materials. The particles were evaluated in a powder bed configuration. This setup was chosen to isolate the effects of particle morphology control without the influence of binder or processing variables and serves as a model system for understanding the fundamental material behavior. Glass was selected because of its high degree of freedom in forming particles directly from the melt. In addition, glass compositions adapted to the battery environment provide a reasonable alternative to the particles that are currently used in battery applications. The material density is significantly lower than that of ceramics such as alumina. Furthermore, glass exhibits superior thermal stability compared to polymers or boehmite (Figure S1).

The schematic morphology of a glass flake compared to the real morphology obtained by SEM is shown in Figure 1.

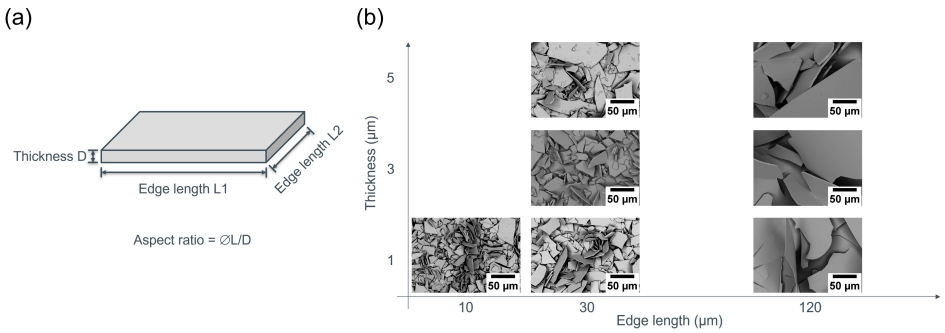

Figure 1. Characteristics of platelet-shaped particles: (**a**) Labeled schematic with size specifications; (**b**) SEM micrographs of differently sized glass flakes.

Although L1 and L2 are in the same range, they do not necessarily possess the same value. Consequently, the morphology of glass flakes can vary considerably, exhibiting shapes such as square, rectangular, or even needle-like structures, depending on the manner of their fragmentation during milling. The most important attribute for the description of platelet-shaped particles, such as glass flakes, is the aspect ratio, which is defined as the ratio between edge length and thickness (L:D).

To investigate the influence of the two factors, particle fractions at high and low levels of thickness and edge length are compared. Furthermore, particles of fixed thickness and varying aspect ratio are selected. In order to provide a reference point, the edge length of a fraction of glass flakes was deliberately reduced as much as possible by excessive ball milling to reduce the aspect ratio and eliminate the platelet shape. The composition of the glass flakes is provided by the manufacturer and is included in the Supporting Information (see Table S2).

To demonstrate the thermal stability of battery separator materials, commercially available boehmite (γ-AlOOH) particles and a polypropylene separator (Celgard®, Polypore International, Charlotte, NC, USA) were selected as references.

2.2. Cell Assembly and Cycling

All cells for the electrochemical characterization were assembled in an argon-filled glove box (O_2 and H_2O content < 1 ppm) in a coin-cell-type setup (Swagelok cell, Supporting Information Figure S2).

In order to conduct electrochemical impedance spectroscopy of the glass powders, stainless steel electrodes were employed. Prior to sealing, defined bulk powder volumes were placed within the cell and compressed. The height of the powder beds was adjusted and verified by measuring the height of the cells before and after assembly.

Symmetric cells with 12 mm coins of pure lithium metal (750 µm, Alfa Aesar, Haverhill, MA, USA) were used to test the dendrite suppression capability of glass flakes. For this cell type, in addition to the powder bed, a Whatman GF/C glass-fiber non-woven (Cytiva, Wilmington, DE, USA) with a diameter of 12.5 mm was placed to avoid immediate short circuiting due to possible displacement of the particles. The glass-fiber non-woven also served as reference separator for this test.

Half-cells were assembled to test the effective capacities when using a powder bed as a separator. To build graphite–lithium cells in half-cell configuration a commercially obtained graphite-coated copper foil (Customcells Itzehoe GmbH, Itzehoe, Germany) was used as electrode (spec. capacity: 355 mAh g^{-1}). Furthermore, a 12 mm coin of pure lithium metal served as counter electrode.

Prior to cell assembly, the graphite electrodes were punched out to 12 mm coins and dried at 110 °C for 16 h together with the glass flakes in Argon atmosphere. To maintain a constant pressure (0.05 MPa), a steel spring (EN material number: 1.4310, Gutekunst springs, Metzingen, Germany) and a nickel coin (d = 12 mm, h = 500 µm; HMW Hauner, Röttenbach, Germany) were placed inside the cell stack.

For all the cells a 1 M solution of $LiPF_6$ in a 1:1 (v/v) mixture of ethylene carbonate (EC) and dimethyl carbonate (DMC) (Selectilyte^{TM} LP 30, BASF, Ludwigshafen, Germany) was used as the electrolyte.

2.3. Physico- and Electrochemical Characterization Techniques

2.3.1. Microstructural Evaluation

The scanning electron microscopy (SEM) characterization shown in this study was performed using a Zeiss scanning electron microscope (LEO 1530, Zeiss, Jena, Germany) at an accelerating voltage of 5 kV. The glass particles were characterized by SEM to reveal their microstructure and illustrate the different aspect ratios.

The nominal particle size of the glass flakes was verified by laser diffraction technology using a particle size analyzer (PSA 1190, Anton Paar, Graz, Austria).

The specific surface area of the particle fractions was determined by N_2 physisorption (ASAP 2010, Micromeritics, Unterschleißheim, Germany) according to Brunauer-Emmet-Teller (BET).

2.3.2. TGA

Thermogravimetric analysis (NETZSCH STA 449 F5 and 449C, Selb, Germany) was conducted up to 700 °C in nitrogen atmosphere (heating rate 5 K min^{-1}; gas flow 45 mL min^{-1}).

2.3.3. Mechanical Characterization

Mechanical testing was performed using a universal testing machine (inspekt duo 10, Hegewald & Peschke, Nossen, Germany). The aspect ratio-dependent penetration resistance of particle layers was determined in close accordance with the standard ASTM F 1306 using a Swagelok setup [37]. Prior to penetration, 0.5 g of glass particles were compacted at 10 MPa for a period of 1 min. Subsequently, an indenter with a tip radius of 1.6 mm and a conical shaft with an inclination of 6° was driven into the particle bed, and the resistance force was measured with a 500 N load cell. The testing device was set to a traverse speed of 1 mm min^{-1}. The termination criterion was reached at a measured force of 20 N. For the calculation of penetration resistance, the gradient of the force measurement curve is determined in the linear-elastic range of the force measurement graph. In this region, the particle layer is supported by interlocking of the particles before either lateral displacement or excessive compaction occurs. This provides a parameter analogous to the modulus of elasticity, which enables comparison of the particles with varying morphologies, i.e., aspect ratios.

2.3.4. Linear Sweep Voltammetry

The electrochemical stability of the particles soaked with liquid electrolyte was investigated by carrying out linear sweep voltammetry (VMP3, Biologic, Seyssinet-Pariset, France) experiments utilizing stainless steel electrodes. These experiments were conducted within a potential range of 0.0–5.0 V at a scanning rate of 0.02 mV s^{-1}.

2.3.5. Electrochemical Impedance Spectroscopy (EIS)

Conductivity measurements were performed at 23 °C using galvanostatic impedance spectroscopy (Reference 600, Gamry Instruments, Warminster, PA, USA) from 1.0 MHz to 0.5 Hz with an AC current of 0.1 mA. Each sample was measured three times in a Swagelok

cell setup with stainless steel electrodes. The ionic conductivities were then calculated, taking into account the internal resistance, thickness and area of the particle layer.

The objective of this analysis was to evaluate the effect of two factors (edge length and thickness) at two levels on the ionic conductivity of electrolyte-soaked powder beds containing glass flakes of different aspect ratios. This was achieved by the implementation of a full factorial design of experiments.

2.3.6. Galvanostatic Cycling

Further electrochemical investigations of the cells were carried out at 23 °C using a BaSyTec CTS Lab (Asselfingen, Germany) battery tester after a 24 h rest period following cell assembly.

Li-Li symmetric cell cycling was performed in a galvanostatic mode after a formation step at 0.25 and 0.5 mA cm^{-2} for two cycles each, until an areal capacity of 1.0 mAh cm^{-2} was reached. Subsequently, a constant current density of 1.0 mA cm^{-2} was applied for 100 cycles, followed by an increase to 2.0 and 3.0 mA cm^{-2} for 100 cycles each.

The galvanostatic cycling protocol for all tested half-cells started with a formation procedure (two cycles at C/10; two cycles at C/5; one cycle at C/2). After an additional 15 cycles at C/2 the current density was gradually increased to 1C, 2C and 5C (five cycles each), followed by another five cycles at C/2 to evaluate the effects of high current densities on the accessible capacity of graphite–lithium half-cells. The discharge and charge conditions were maintained in constant current mode, with a cut-off voltage of 0.01 V and 1.0 V, respectively.

3. Results and Discussion

In order to further improve the safety of lithium-ion batteries, the advantages of platelet-shaped particles are compared with those of arbitrarily shaped particles. The use of these so-called glass flakes serves the purpose of forming an effective barrier against growing lithium dendrites by establishing a self-stabilizing structure, as illustrated in Figure 2. This barrier prevents or at least effectively delays the piercing of the separator [15].

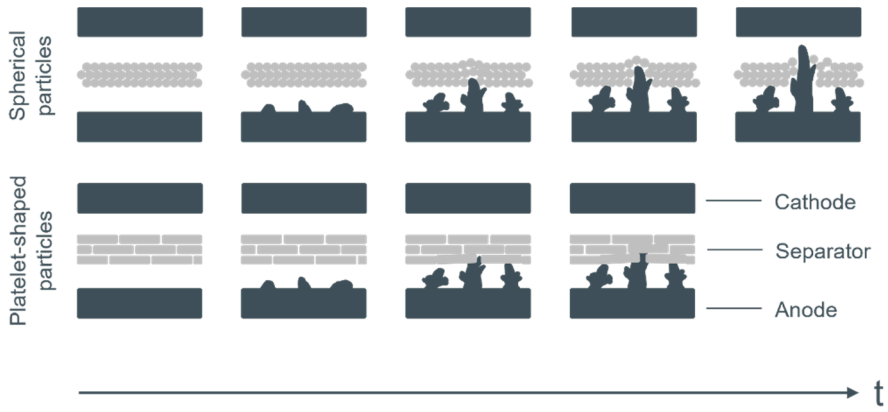

Figure 2. Schematic representation of the progressive propagation of dendrites in two different types of separators: spherical particle layers compared to "brick-and-mortar structure" of platelet-shaped particles under piercing stress.

The outcome of this fundamental research, employing particles in powder bed configuration, is expected to provide guiding significance for practical application of particle-based separators.

3.1. Size and Morphology of the Different Glass Particles

The thickness of the glass flakes is determined by the selected production parameters such as the viscosity of the melt and the rotational speed of the crucible, while the edge length is adjusted by milling and classifying. This allowed the characteristics of the separator to be tailored by selecting the optimum flake size.

Microstructures of glass flakes with different edge lengths but equal thickness of 1 µm, i.e., different aspect ratios, were evaluated by scanning electron microscopy and are shown in Figure 3. The glass flakes with varying edge length and thickness, used to determine the effects of these parameters by full factorial design of experiments, are illustrated in the Supporting Information (Figure S3).

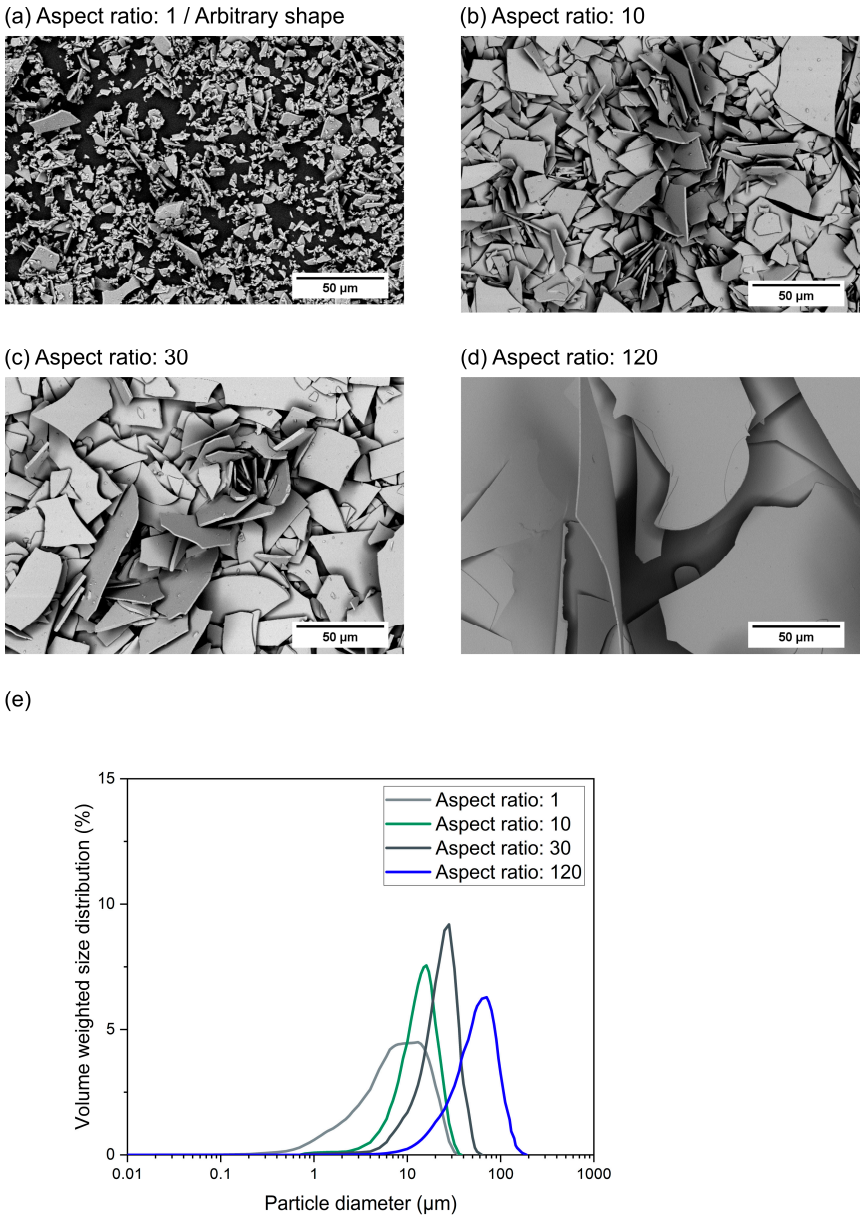

Figure 3. SEM images of glass flakes with aspect ratios of (**a**) 1; (**b**) 10; (**c**) 30; (**d**) 120 corresponding to a thickness of 1 µm and (**e**) their respective particle size distribution.

All glass particles have a sharp-edged morphology devoid of any discernible agglomerations. The glass flakes display a rectangular appearance, with one edge length falling within the range of the nominal edge length, while the other edge exceeds it. The particles range from powder-like structures at low aspect ratios to platelets with a medium aspect

ratio, and sheet-like morphologies at high aspect ratios. The preferred fracture mode of the glass platelets is along the edges, with minimal impact on the thickness, resulting in a cube-like appearance after milling [38]. Some residual platelet-shaped particles are also present. No sieve classification could be conducted in this size range due to the unavailability of sieves with a mesh size of less than 10 microns.

The determination of a mean particle size of the platelets is challenging due to the fact that the measured values represent a mixture of the expansion obtained in each spatial direction, resulting in a wide distribution [39]. However, the characteristic particle sizes determined by laser diffraction are in accordance with the data sheet (Table 1) and the SEM images. The distribution of the milled particles is the broadest observed, which is due to the partially incomplete milling and classifying, respectively.

Table 1. Geometric properties of the particles with a thickness of 1 µm and varying edge length.

Sample	GF001 Milled	GF001-10	GF001	GF100M
Nominal aspect ratio	1	10	30	120
D10 (µm)	1.81	5.98	9.97	22.46
D50 (µm)	7.14	12.95	22.09	53.83
D90 (µm)	17.06	20.72	34.41	93.35
Specific surface area ($m^2\ g^{-1}$)	1.01	0.81	0.71	0.29

As the particle size is reduced, the specific surface area of the particle collective increases, while maintaining a relatively moderate level in comparison to that of common separator materials.

3.2. Penetration Resistance Test of Platelet-Shaped Particle Layers

The ability of battery separators to resist piercing by lithium dendrites is a crucial attribute for their intended application. The depth-dependent force for penetration into a compacted particle bed is regarded as a measure of the beneficial effect of platelet-shaped particle modification of separators on their penetration resistance. While the macro-scale puncture test cannot directly mimic the electrochemical process of micro-scale lithium dendrite growth, it is nevertheless considered to serve as an indicator of bulk mechanical strength. This initial assessment of the structural robustness of the flake layers may be correlated with the capability to avoid penetration-related shorting [7,40].

Figure 4 illustrates the depth-dependent penetration resistance of glass particles with a thickness of 1 µm with respect to the aspect ratio of the particles.

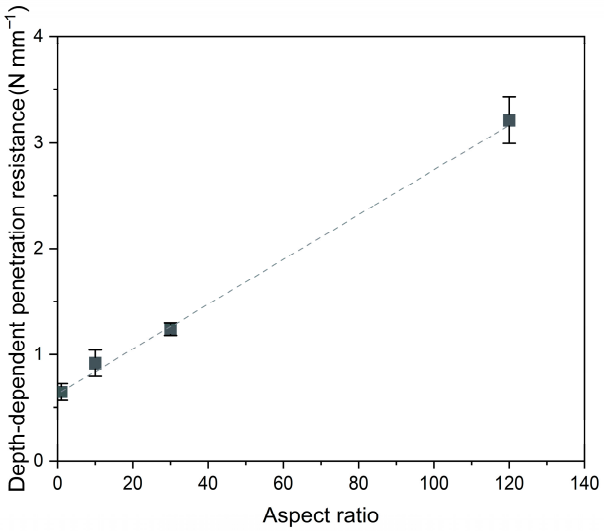

Figure 4. Penetration resistance of particle layers as a function of particle aspect ratio.

The penetration resistance of particle layers increases linearly with the aspect ratio of the particles. Consequently, a bulk sample of glass would invariably demonstrate the highest penetration resistance—but battery separators need to be flexible for the battery assembly process, which often involves processes such as winding, where a high degree of curvature is applied. The use of particulate systems is therefore essential. A direct comparison between these experimental values and the puncture resistance of separator foils is not feasible, as the latter represents a continuous phase. Nevertheless, the penetration resistance of the powder beds still serves to illustrate the stabilizing effect of an increasing edge length of the particles. We propose that the utilization of platelet-shaped particles with an optimized aspect ratio will allow for flexible processing and, at the same time, markedly enhance the penetration resistance, demonstrating the barrier effect of platelet-shaped particles.

We assume that the increase in penetration resistance with increasing aspect ratio is attributed to the increasing edge length of the particles, while maintaining a constant thickness of 1 µm. This results in a greater number of regions exhibiting particle overlap, a phenomenon that is particularly evident in sheet-like particles such as the platelets utilized in the present study. Consequently, more efficient lateral load spreading and vertical load transmission are facilitated, thereby enabling effective stress propagation with increasing aspect ratio. These mechanisms can also be observed for impact load spreading in other layered structures [41–43]. In general, particles with a low aspect ratio tend to exhibit less displacement under stress, which can reduce their probability of fracture when subjected to penetrating forces. As a result, these particles are simply pushed aside by the penetration needle in our experimental setup or the dendrite in the battery. Particles with high edge lengths are more effectively fixed due to the formation of entanglements among these particles. Moreover, when the applied strain exceeds a certain limit, the particles tend to fracture, leading to energy dissipation. These mechanisms are similarly implemented by Liu et al. and Guo et al. to impede dendrite growth in other battery types [44,45]. Furthermore, a high mechanical strength of the particle layers can offer a significant advantage for cells that comprise silicon as anode material. As described by Seo et al., this indicates a method of mitigating the mechanical shutdown caused by the volume expansion of silicon particles, which is ultimately culminating in a structural collapse of the separators' porous structure [4].

3.3. Long-Term Stability of Symmetric Li-Li Cells

While the mechanical barrier function of platelet-shaped glass particles has been proven, the significance of this physical property in an electrochemical environment is further investigated by the cycle life of symmetric Li-Li cells containing glass particles in powder bed configuration, together with a glass-fiber non-woven reference separator. The formation of high-surface area lithium constitutes a safety issue [46]. Cell assembly was conducted according to Koo et al. with the objective of facilitating the growth of dendrites on the lithium electrode in direct contact with the particles [47]. The dendrite suppression capability of those particles can thus be experimentally demonstrated by prolonged cycle life, homogeneous voltage profiles and low voltage polarization even at increasing current densities. Based on the mechanical testing, high cycle stability is expected in the cells containing particles with a high aspect ratio. This expectation is however proven wrong by the cycling data in Figure 5. Here, we find that an aspect ratio of 120 leads to fatal cell failure after only a few cycles, although this aspect ratio was previously identified as the one that provided the highest mechanical strength. In order to ensure clarity of the graph, a termination criterion of $\pm$0.5 V for more than 5 min was established for the evaluation. The complete illustration of the data can be found in the Supporting Information (Figure S4).

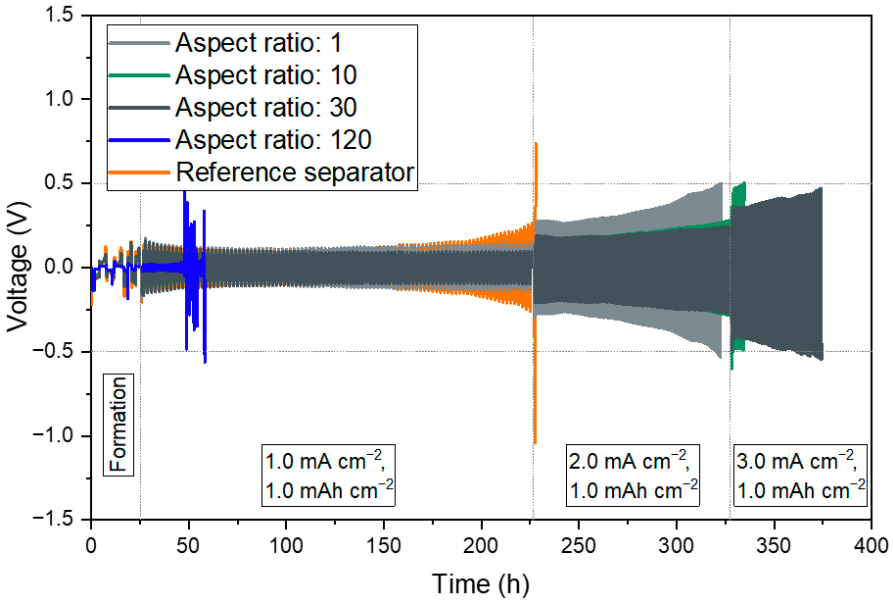

Figure 5. Galvanostatic voltage profiles of Li-Li symmetric cells with a capacity of 1 mAh cm^{-2} and a termination criterion at ±0.5 V employing particle bed separators with varying aspect ratios.

Following the formation cycles, galvanostatic charge–discharge testing was initiated at a current density of 1.0 mA cm^{-2} and an areal capacity of 1.0 mAh cm^{-2}. As expected, the initial voltage polarization of the reference cell is the lowest observed, as there is no additional particle layer involved. Nonetheless, after approximately 150 h the voltage polarization was deteriorating considerably, reaching the termination criterion of ±0.5 V for more than 5 min after a higher current density was applied. The highly porous structure of the Whatman GF/C non-woven reference separator, with a median pore size of 1.2 µm, limits its applicability to current densities of 1.0 mA cm^{-2} and below. The extended illustration in Figure S4 also reveals a sudden voltage drop after a few more cycles, indicating subsequent short-circuiting of the cell [48,49].

The data also indicates that separator particles with a high aspect ratio of 120 lead to inhomogeneous cycling and high voltage polarization exceeding the limit of ±0.5 V already after a limited number of cycles at the initial current density for cycling. In contrast, the overpotential of cells protected by a particle layer of an aspect ratio of 1, 10 and 30 is relatively stable over 200 h (100 cycles) at a current density of 1.0 mA cm^{-2} after formation, as shown in Figure 5. However, upon increasing the current density to 2.0 mA cm^{-2}, the voltage of the cell containing arbitrarily shaped particles (aspect ratio: 1) rises exponentially to over 0.5 V, resulting in the termination after 96 cycles at this rate. In contrast, the voltage polarization of the cells with particles of a moderate aspect ratio (10 and 30) increased to only around 0.25 V after the full 100 cycles at 2.0 mA cm^{-2}, which is significantly less pronounced. The improved cycle and rate stability exhibited by the particles with an adapted aspect ratio demonstrates the robustness that a glass particle separator layer can provide in the long-term operation of lithium cells [50]. As the current density further increased to 3.0 mA cm^{-2}, the voltage polarization of both remaining cells also increased, approaching the termination criterion after 214 and 274 cycles, respectively.

It is shown that the implementation of glass particles as separator can facilitate an effective barrier, enabling the stable cycling of lithium batteries. This enhancement is particularly noteworthy when compared to the performance of a reference separator. However, the effectiveness of the particles depends on their aspect ratio. Only the particles with moderate aspect ratios of 10 and 30, respectively, enabled long-term cycling even at elevated current densities. An aspect ratio that is too low provides less stability at elevated

current densities. Conversely, a too high aspect ratio inherently results in excessive voltage polarization and inhomogeneous ion transport. This provides experimental evidence to support the phase-field simulation models proposed by other researchers [27,45].

These results are, though, in contrast to the determined mechanical penetration resistance, which increases proportionally with the aspect ratio of the particles. This implied that the highest cycling stability would be achieved at the highest aspect ratio. Our findings demonstrate that this is not the case for symmetrical lithium cells. The penetration resistance of particle layers as measure for the robustness of particle-based battery separators might be applicable for anode materials that exhibit directed volume expansion like silicon, as reported by Seo et al. in their study of mechanical shutdown [4]. However, this principle may not extend to materials that form dendritic structures by volume modulation like lithium metal. Accordingly, the suppression of dendrite growth does not only rely on the mechanical strength of the barrier layer, but also on the interplay of additional influencing factors, such as deposition kinetics and nucleation potential to guide the uniform deposition of lithium [51]. The influence of these factors is discussed in the relevant literature [52–54]. Also, the tortuosity and porosity of the separator may impact the behavior of the cell [55,56]. In order to verify the underlying mechanisms behind these observations, the electrochemical stability and the ionic conductivity of the powder beds in contact with the battery electrolyte are subsequently evaluated.

3.4. Electrochemical Stability

Linear sweep voltammetry (LSV) was performed to determine the electrochemical stability dependent on the particle material (see Figure 6). The glass particles were compared to commercial boehmite (γ-AlOOH) particles.

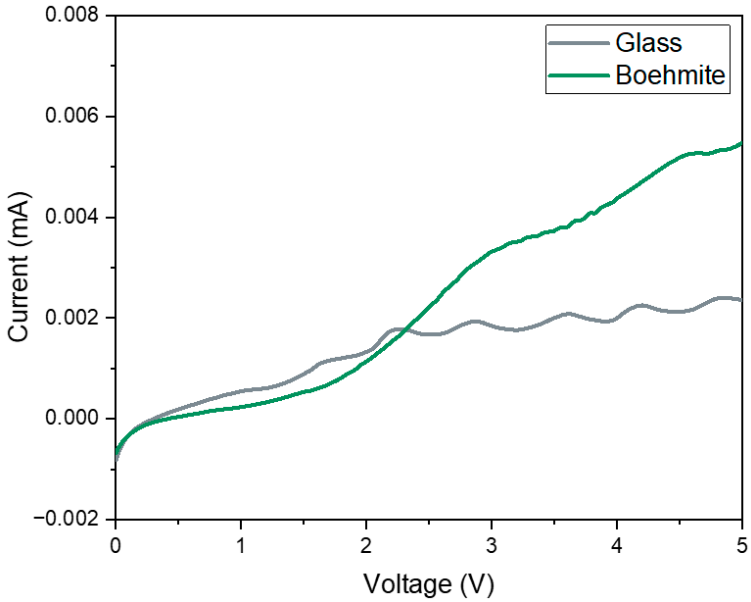

Figure 6. Linear sweep voltammetry (LSV) curves of particles in a 1 M solution of $LiPF_6$ in a 1:1 (*v*/*v*) mixture of ethylene carbonate (EC) and dimethyl carbonate (DMC).

The LSV curves of glass and boehmite particles for reference exhibit a comparable shape. Their currents are below 2 µA for glass, which is even lower than for boehmite (6 µA), indicating that no redox reaction takes place in the system below 5.0 V. Consequently, when these cells are operated within the typical voltage range of 2.5–4.5 V, the glass particles are stable and can meet the requirements of lithium-ion battery operation. The measured current of the glass particles showed minimal variation across the potential window, even lower than that of the boehmite. These results indicate that the glass particles do not only possess electrochemical stability when operated within the relevant voltage range for

the intended application but also have a reduced propensity for side reactions compared to boehmite.

3.5. Effect of Particle Size and Shape on Ionic Conductivity in Liquid-Electrolyte Systems

A full factorial design of experiments was employed to evaluate four different fractions of particles, characterized by two levels of thickness (1 µm, 5 µm) and edge length (30 µm, 120 µm), with respect to the ionic conductivity of a liquid electrolyte-soaked bulk powder bed containing these particles. Since the glass particles are non-conductive, the electrolyte phase is the sole contributor to ionic conductivity. Liquid electrolyte is soaked up in the voids and the resulting conductivity is dependent on the distribution and connectivity of the percolating phase as well as the porosity and tortuosity of the particle layers. The ionic conductivities calculated from impedance measurements for each combination are given in Table 2.

Table 2. Evaluation of the effect of thickness and edge length of platelet-shaped particles on the ionic conductivity of an electrolyte-soaked powder bed containing these particles.

Flake Type	Thickness (µm)	Edge Length (µm)	Ionic Conductivity (mS cm^{-1})
1	1	30	3.157
2	5	30	3.350
3	1	120	0.195
4	5	120	1.025
Contrast	1.0230	−5.2870	
Effect	0.5115	−2.6435	

The effect of the "Thickness" parameter is slightly positive, meaning that increasing the flake thickness slightly improves the ionic conductivity of the powder bed. In contrast, the effect of the "Edge length" parameter is strongly negative, i.e., increasing the edge length of the flakes strongly reduces the ionic conductivity of the powder bed. This is consistent with the screening of different flake types in Figure 7a.

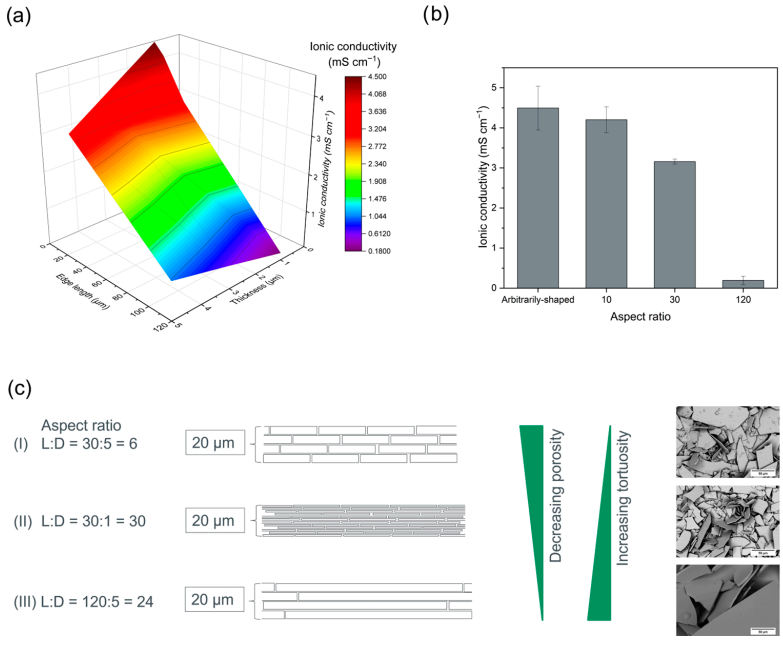

Figure 7. Ionic conductivity of electrolyte-soaked particle layers: (**a**) Heatmap of the ionic conductivity of powder beds with platelet-shaped particles of varying edge length and thickness; (**b**) Ionic conductivities of powder bed separators with particles of different aspect ratio; (**c**) Scheme of the effect of particle thickness and edge length on the structural composition and properties of perfectly layered separators with given thickness.

The lowest ionic conductivity is obtained with particles of high edge length and low thickness, while a powder bed of particles of low edge length and high thickness provides the highest ionic conductivity. The influence of the edge length is significantly higher than the influence of flake thickness. It can be concluded that a high aspect ratio reduces the ionic conductivity.

We consider the influence of thickness and edge length using a thought experiment. A few assumptions are made to illustrate this. The fixed height of the battery separator is 20 µm. In addition, a brick-and-mortar structure is assumed due to the flat orientation of the flakes and the presence of a homogeneous layer structure.

The developed influencing factors of the platelet size and aspect ratio on the ionic conductivity in a non-aqueous battery electrolyte are visualized in Figure 7c. The brick wall modelling clearly shows that for thin particles with short edge lengths there is a high porosity with moderate tortuosity. The porosity of the system is determined by the edge length of the particles, which defines the number of "entrances" for the Li^+ ions. The tortuosity is represented by the distance that needs to be covered to pass the glass particle layer for a given total thickness. This distance increases with decreasing particle thickness (see (I) and (II) in Figure 7c). If the edge length of the particles is too high, the accessibility for Li^+ ions is blocked, and the ionic conductivity is low as shown in (III) in Figure 7c. Based on these findings, we again attribute the main influence on the electrochemical performance to the edge length of the particles. The fact that the thickness of the glass flakes has only a minor influence is advantageous for the flake processing, as the edge length can easily be adjusted by milling. In addition, thinner particles are beneficial for the volumetric energy density of battery cells because they allow lower separator thickness for a given number of particle layers. Accordingly, the following considerations are constrained to particles with a constant thickness of 1 µm and varying edge lengths and aspect ratios, respectively.

The ionic conductivities of the powder beds with 1 µm thick flakes and varying aspect ratios (as shown in Figure 3) are compared in Figure 7b. The arbitrarily shaped particles with an aspect ratio around 1 were obtained by excessive milling of glass flakes to eliminate the platelet shape. Particle layers with low aspect ratios of 1 and 10 exhibit an ionic conductivity of approximately 4.5 mS cm^{-1}. A slight decline is observed at an aspect ratio of 30, followed by a significant drop at a high aspect ratio of 120. This substantiates the concept of the brick-and-mortar structure hypothesis introduced in Figure 2 and aligns well with the cycling data presented in Figure 5. The planar morphology of these platelets impedes lithium-ion transport by blocking access points to the separator layer, increasing the diffusion path length and hindering ion transport.

On the other hand, the decrease in ionic conductivity between arbitrarily shaped particles and flakes with an aspect ratio of 10 is negligible. Therefore, maintaining the indicated barrier function by using glass flakes with short edge lengths instead of arbitrary shapes is a viable option, which is also consistent with the size ratio of those heterogeneous blocks used to mitigate dendrite propagation in the phase-field based multiphysics model of Yuan et al. [27]. However, a further increase in the glass flake size is not recommended, because the ionic conductivity decreases rapidly when the aspect ratio is greater than 10.

3.6. Accessible Capacity in Graphite–Lithium Half-Cells

To gain insight into the accessible capacities of graphite–lithium half-cells containing separators made of glass platelet layers with varying aspect ratios, the cell voltage over the specific capacity in the first lithiation step is compared for given C-rates in Figure 8. Half-cells were utilized to isolate the effects of the morphology of the separator particles without the added complexity of full-cells as the current study focuses on the fundamental behavior of

the separator material. Electrochemical performance data of batteries using the reference separator (Whatman GF/C) can be found in the Supporting Information (Figure S5).

(a)

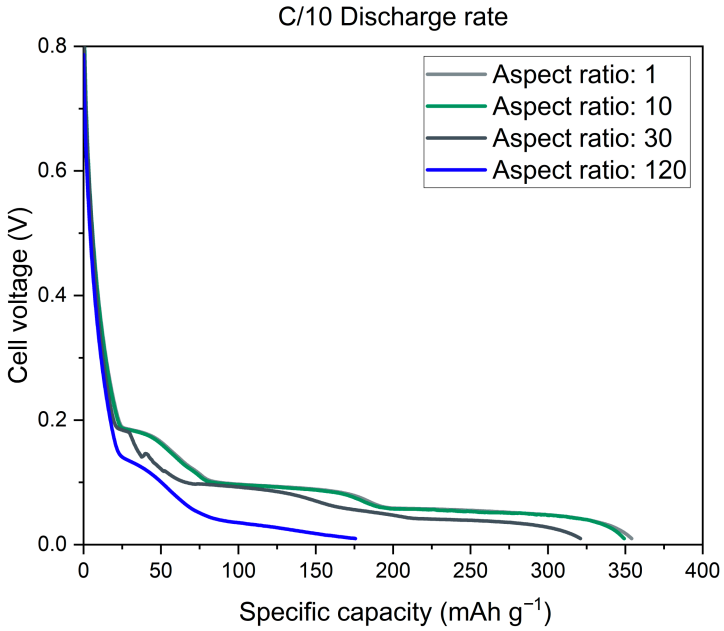

(b)

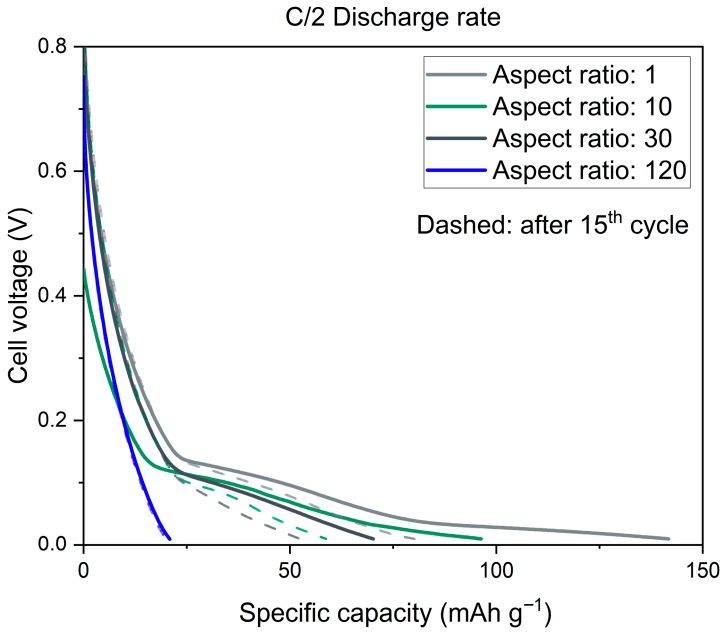

Figure 8. Cell voltage vs. capacity recorded during a constant current discharge at (**a**) C/10 (1st cycle); (**b**) C/2 (1st and 15th cycle).

The accessible capacities in lithium half-cells vary significantly for the different aspect ratios. The initial lithiation of the graphite anode has been evaluated, demonstrating that at low discharge rates, such as C/10 in Figure 8a, almost the entire specific capacity of the electrode material graphite (372 mAh g^{-1}) can be utilized with separator layers of particles with an aspect ratio of 10 or lower [57,58]. The following capacities have been achieved:

354 mAh g^{-1} at aspect ratio 1, 349 mAh g^{-1} at aspect ratio 10, 321 mAh g^{-1} at aspect ratio 30 and 175 mAh g^{-1} at aspect ratio 120.

Accordingly, the accessible capacity of the electrode is clearly limited by the morphology of the separator particles when a voltage-related termination criterion (0.01 V) is employed. The utilization of flakes with an aspect ratio of 10 or lower as a separator has resulted in twice the capacity compared to an aspect ratio of 120, at a discharge rate of C/10.

As shown in Figure 8b, the accessible capacities decline significantly at an elevated discharge rate of C/2 for all aspect ratios considered in this study. This is a direct consequence of using bare glass particles in their natural state, without any additional processing to enhance their suitability as separators, such as surface treatment or grafting. Nevertheless, the influence of the aspect ratio is clearly visible. It is evident that at a discharge rate of C/2, the difference in accessible specific capacity among the various aspect ratios is even more pronounced. In this instance, the capacity is three times higher when using flakes with an aspect ratio of 10 compared to those with an aspect ratio of 120, and almost five times higher when using flakes with an aspect ratio of 1 as separator. It is also notable that the ratio between $C_{lith,C/2}$ and $C_{lith,C/10}$ gives a first impression of the rate capability of the cells. For example, the capacity at C/2 is only 27.5% of the initial capacity at C/10 for an aspect ratio of 10 and even lower for higher aspect ratios.

All the specific capacities related to the mass of active material and the proportion of the remaining capacity at elevated C-rate are summarized in Table 3.

Table 3. Comparison of the electrochemical values of the presented particle morphologies.

Sample	Aspect Ratio 1	Aspect Ratio 10	Aspect Ratio 30	Aspect Ratio 120
C_{lith} (1st cycle at C/10) (mAh g^{-1})	354	349	321	175
C_{lith} (1st cycle at C/2) (mAh g^{-1})	142	96	70	21
C_{lith} (15th cycle at C/2) (mAh g^{-1})	80	59	52	20
$C_{lith,C/2,15th}/C_{lith,C/2,1st}$ (%)	56.3	61.5	74.3	95.2
$C_{lith,C/2,1st}/C_{lith,C/10,1st}$ (%)	40.1	27.5	21.8	12.0

In order to investigate the stability of the electrochemical performance over time, the accessible capacity is once again monitored at the 15th discharge cycle. Now the particle fractions that demonstrated a high initial performance exhibit the highest degree of degradation. After 15 cycles at C/2 the cells with particles of an aspect ratio of 1 reach only 56.3% of their initial capacity, while the quotient $C_{lith,C/2,15th}/C_{lith,C/2,1st}$ is 95.2% for an aspect ratio of 120. Flakes with an arbitrary shape (aspect ratio of 1) still remain the optimum choice for achieving high capacity, while particles with an aspect ratio of 10 and 30 demonstrate comparable performance at a level below that of the aforementioned particles. However, the performance of these particles is also subject to capacity fade. While this is less severe, it is still a significant issue and suggests that a higher aspect ratio alone does not fully prevent long-term instability. The increased susceptibility to degradation can be explained by the specific surface area of those various particle fractions shown in Table 1. Greater propensity for side reactions during galvanostatic cycling is the result of an increase in surface area. This encompasses surface-related phenomena, including side reactions at the glass surface, alterations to the surface morphology, an increase in contact angle between separator and electrolyte, as well as pore blockage caused by electrolyte evaporation and salt precipitation [59,60]. The volumetric quantity of electrolyte was constant for each cell, resulting in a reduction in the available amount of electrolyte per overall particle surface area with increasing particle-related surface area. The drying-out of the electrolyte over time led to a decline in the electroactive surface area and the volume

fraction of active material and accelerated capacity fading, as described by Fang et al. [61]. Thus, the effects of capacity loss after long-term cycling are less pronounced with the lower surface area at an aspect ratio of 120. These results highlight the potential for optimization through surface modification or by integrating the particles into a composite structure to enhance long-term electrochemical stability.

3.7. Influence of Flake Geometry on Fast Charging Behavior

High-rate capability of lithium-ion batteries represents a significant challenge in the field of battery research. In particular, separator modification with non-porous and non-ion-conductive particles could potentially compromise battery performance. Therefore, the battery's fast charging behavior is analyzed by incrementally increasing the charging currents. Again, layers of glass flakes with different aspect ratios are used as separators in a half-cell configuration (graphite/lithium). Figure 9a illustrates the relative capacity in relation to the first cycle at C/2, with data points representing 1C, 2C and 5C each comprising five cycles. The subsequent recovery of the initial capacity is highlighted by an additional five cycles at C/2 following the C-rate variation.

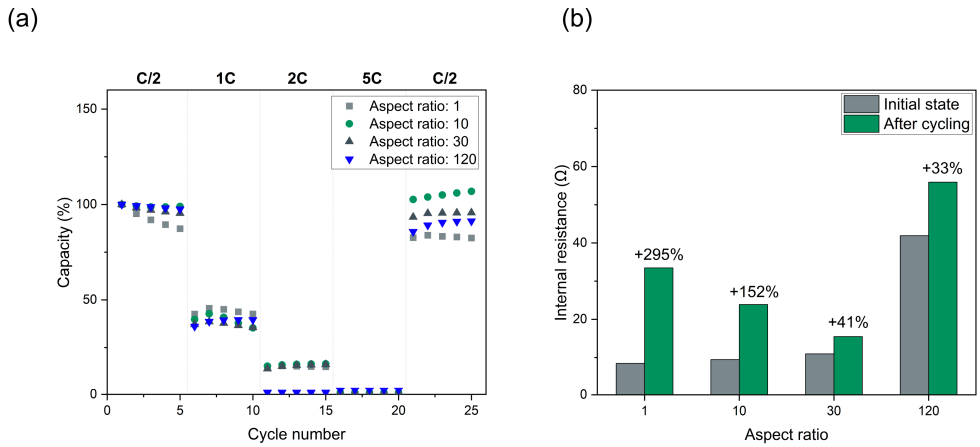

Figure 9. Charging behavior of graphite–lithium half-cells: (**a**) Capacity retention during C-rate variation using platelet-shaped glass particles as separator material; (**b**) Comparison of the internal resistance for particle-bed separators with varying aspect ratios.

The obtained results are in good agreement with the respective ionic conductivities. Particles with an aspect ratio too high, such as those with L:D = 120, impede the Li^+ diffusion pathways, leading to lower performances. This is particularly evident at elevated C-rates. While the relative reduction in capacity is consistent across all aspect ratios at 1C, there is no usable capacity at 2C with high aspect ratio particles. All unprocessed particle layers reached their limit at 5C, with all samples failing to charge at this point. Therefore, the enhanced ionic conductivity of particle layers consisting of flakes with short edge lengths is particularly advantageous for fast-charging applications.

The subsequent recovery of capacity to the initial value before the C-rate variation is complete for aspect ratio 10, but incomplete for aspect ratios 1, 30 and 120, respectively. This finding suggests that the rapid polarization during incomplete fast charge and discharge cycles may have compromised the structural integrity of the cell. Such a scenario could potentially result in phenomena such as lithium plating or electrolyte decomposition, which in turn would obstruct the electrode surface. If the aspect ratio is too low, the brick wall-like safety barrier cannot be formed in its entirety. If the aspect ratio is too high, the internal resistance, combined with high currents can compromise the integrity of the electrode material.

A comparison of the internal resistance of the half-cells before and after cycling, as illustrated in Figure 9b, serves to confirm the phenomenon of accelerated degradation at low

separator particle aspect ratio. The half-cells with glass particle-bed separators demonstrate an increase in internal resistance following cycling with C-rate variation for all types of glass flakes. The degree of degradation is defined by the relative increase in internal resistance. It is therefore evident that a low aspect ratio, which may be characterized by a high specific surface area, allows for a greater number of side reactions to occur, as mentioned above, which in turn leads to the observed decline in electrochemical performance.

Despite the promising trends observed, we acknowledge the limitations of the current powder bed and half-cell configuration and the need for further validation in more application-relevant formats to fully represent commercial battery conditions. These constraints were intentionally chosen to isolate the effects of particles, as this study focuses on the fundamental influence of particle morphology on separator performance. It is worth mentioning that the particles are used as received without any processing steps to enhance their suitability. The observed behavior may also depend on the material and glass composition. However, as the focus of this study was the influence of particle morphology, the long-term stability will be considered in further studies. The same applies to the influence of binder and coating parameters to extend the experimental results to actual thin battery separators.

To more directly assess application relevance, future work will explore the integration of platelet-shaped glass particles into scalable separator architectures like polymer matrices. Also, full-cell validation with standard cathode materials represents an important step in the development of application-ready separators.

4. Conclusions

This study presents a systematic investigation into how the aspect ratio of platelet-shaped glass particles influences separator performance in lithium-ion batteries. By using a controlled powder bed configuration, we isolated the effect of particle morphology on ion transport, mechanical resistance, and electrochemical behavior. The hypothesis of using a barrier similar to a "brick-and-mortar structure" made of glass platelets, also referred to as glass flakes, in order to toughen separators mechanically has been experimentally tested and proven correct.

As demonstrated by the symmetric cell cycling data, this can indeed facilitate the stable cycling of lithium batteries. This is particularly relevant for cells utilizing volume-expanding materials like silicon anodes. However, only the particles with a moderate aspect ratio enabled long-term cycling even at elevated current densities. An aspect ratio that is too low provides less stability at elevated current densities. On the other hand, an excessively high aspect ratio leads to uncontrolled voltage polarization and inhomogeneous ion transport.

Accordingly, it was found that the design of particle-based separators can be tailored to specific application requirements by the aspect ratio of the particles. Galvanostatic cycling tests were performed in a half-cell configuration with a variation in C-rate to evaluate the influence of separator particles on the accessible capacity of graphite electrodes. While the aspect ratio of particles has a relatively minor impact at low C-rate (C/10) the loss of accessible capacity is significant for particles of high aspect ratio especially at elevated charge current (C/2). This is a consequence of significantly reduced ionic conductivity by blocking the Li^+ diffusion pathways due to the high aspect ratio of the separator particles.

Building on this discovery, the aspect ratio of glass flakes with a thickness of 1 µm was varied by changing their edge length in order to identify an optimum compromise in terms of the electrochemical performance. The ionic conductivity of glass flakes with an aspect ratio of 10 is found to be highly comparable to that of arbitrarily shaped particles with an aspect ratio of 1. Thus, a trade-off between electrochemical performance and safety barrier function was made by choosing particles with a maximum aspect ratio of 10. These

particles represent the optimum choice for ensuring cycling stability, rate capability and capacity retention. Therefore, this work provides a framework for selecting suitable particle sizes and shapes for incorporation into separator materials.

In conclusion, our findings can be readily applied to enhance the characteristics of separators both physically and electrochemically. These insights can support the development of novel particle-based separator concepts that improve the reliability and fast-charging capability of lithium-ion batteries in real-world applications.

Supplementary Materials: The following supporting information can be downloaded at: https://www.mdpi.com/article/10.3390/batteries11110388/s1, Table S1: Sizes of glass platelets used in this study; Figure S1: Thermogravimetric analysis (TGA) curves of typical materials utilized in battery separators; Table S2: Composition of the glass flakes used in this study; Figure S2: Coin-cell-type Swagelok setup used for the electrochemical characterization; Figure S3: SEM images of the glass platelets used in the design of experiments for the determination of the effect of thickness and edge length on ionic conductivity: (a) GF001; (b) GF007; (c) GF100M; (d) GF750M; Figure S4: Galvanostatic voltage profiles of Li-Li symmetric cells with a capacity of 1 mAh cm^{-2} employing particles bed separators with varying aspect ratios; Figure S5: Electrochemical performance data in comparison to using a reference separator (Whatman GF/C): (a) Cell voltage vs. capacity recorded during a constant current discharge at C/10 (1st cycle) and (b) C/2 (1st and 15th cycle); (c) Capacity retention during C-rate variation in half cells; (d) Comparison of the internal resistance of half-cells.

Author Contributions: Conceptualization, P.R.; methodology, P.R. and S.M.; validation, P.R. and S.M.; formal analysis, P.R. and S.M.; investigation, P.R. and S.M.; resources, T.G. and C.R.; data curation, P.R.; writing—original draft preparation, P.R. and S.M.; writing—review and editing, T.G. and C.R.; visualization, P.R.; supervision, T.G. and C.R.; funding acquisition, T.G. and C.R. All authors have read and agreed to the published version of the manuscript.

Funding: The authors thank the Bavarian Research Foundation (Bayerische Forschungsstiftung, BFS; GlasSeLIB—funding code AZ-1463-20) for the funding. Funded by the Open Access Publishing Fund of the University of Bayreuth.

Data Availability Statement: The raw data supporting the conclusions of this article will be made available by the authors on request.

Acknowledgments: The authors would like to thank the Keylab Electron and Optical Microscopy at the Bavarian Polymer Institute (BPI) for SEM imaging (at Zeiss LEO 1530). We would like to thank Lena Geiling (Chair of Electrochemical Process Engineering) for BET-measurements (at ASAP 2010, Micromeritics) and Sven Scheler (Chair of Ceramic Materials Engineering) for the measurement of particle size distributions (at PSA 1190, Anton Paar). Furthermore, P.R. and S.M. thank the graduate school of the Bavarian Center for Battery Technology (BayBatt) for ongoing support.

Conflicts of Interest: The authors declare no conflicts of interest.

References

1. Weber, C.J.; Geiger, S.; Falusi, S.; Roth, M. Material review of Li ion battery separators. In *AIP Conference Proceedings*; American Institute of Physics: College Park, MD, USA, 2014; pp. 66–81.
2. Liu, K.; Liu, Y.; Lin, D.; Pei, A.; Cui, Y. Materials for lithium-ion battery safety. *Sci. Adv.* **2018**, *4*, eaas9820. [CrossRef]
3. Holtmann, J.; Schäfer, M.; Niemöller, A.; Winter, M.; Lex-Balducci, A.; Obeidi, S. Boehmite-based ceramic separator for lithium-ion batteries. *J. Appl. Electrochem.* **2016**, *46*, 69–76. [CrossRef]
4. Seo, J.-Y.; Kim, S.; Kim, J.-H.; Lee, Y.-H.; Shin, J.-Y.; Jeong, S.; Sung, D.-W.; Lee, Y.M.; Lee, S.-Y. Mechanical shutdown of battery separators: Silicon anode failure. *Nat. Commun.* **2024**, *15*, 10134. [CrossRef]
5. Xu, W.; Wang, J.; Ding, F.; Chen, X.; Nasybulin, E.; Zhang, Y.; Zhang, J.-G. Lithium metal anodes for rechargeable batteries. *Energy Environ. Sci.* **2014**, *7*, 513–537. [CrossRef]
6. Kim, S.; Lim, W.-G.; Cho, A.; Jeong, J.; Jo, C.; Kang, D.; Han, S.M.; Han, J.W.; Lee, J. Simultaneous Suppression of Shuttle Effect and Lithium Dendrite Growth by Lightweight Bifunctional Separator for Li—S Batteries. *ACS Appl. Energy Mater.* **2020**, *3*, 2643–2652. [CrossRef]

7. Hao, Z.; Zhao, Q.; Tang, J.; Zhang, Q.; Liu, J.; Jin, Y.; Wang, H. Functional separators towards the suppression of lithium dendrites for rechargeable high-energy batteries. *Mater. Horiz.* **2021**, *8*, 12–32. [CrossRef] [PubMed]
8. Liu, S.; Gu, B.; Chen, Z.; Zhan, R.; Wang, X.; Feng, R.; Sun, Y. Suppressing dendritic metallic Li formation on graphite anode under battery fast charging. *J. Energy Chem.* **2024**, *91*, 484–500. [CrossRef]
9. Wassiliadis, N.; Schneider, J.; Frank, A.; Wildfeuer, L.; Lin, X.; Jossen, A.; Lienkamp, M. Review of fast charging strategies for lithium-ion battery systems and their applicability for battery electric vehicles. *J. Energy Storage* **2021**, *44*, 103306. [CrossRef]
10. Jang, J.; Oh, J.; Jeong, H.; Kang, W.; Jo, C. A Review of Functional Separators for Lithium Metal Battery Applications. *Materials* **2020**, *13*, 4625. [CrossRef]
11. Tan, L.; Sun, Y.; Wei, C.; Tao, Y.; Tian, Y.; An, Y.; Zhang, Y.; Xiong, S.; Feng, J. Design of Robust, Lithiophilic, and Flexible Inorganic-Polymer Protective Layer by Separator Engineering Enables Dendrite-Free Lithium Metal Batteries with LiNi0.8 Mn0.1 Co0.1 O2 Cathode. *Small* **2021**, *17*, e2007717. [CrossRef]
12. Lu, G.; Nai, J.; Luan, D.; Tao, X.; Lou, X.W.D. Surface engineering toward stable lithium metal anodes. *Sci. Adv.* **2023**, *9*, eadf1550. [CrossRef]
13. Xie, Y.; Huang, Y.; Zhang, Y.; Wu, T.; Liu, S.; Sun, M.; Lee, B.; Lin, Z.; Chen, H.; Dai, P.; et al. Surface modification using heptafluorobutyric acid to produce highly stable Li metal anodes. *Nat. Commun.* **2023**, *14*, 2883. [CrossRef]
14. Becking, J.; Gröbmeyer, A.; Kolek, M.; Rodehorst, U.; Schulze, S.; Winter, M.; Bieker, P.; Stan, M.C. Lithium-Metal Foil Surface Modification: An Effective Method to Improve the Cycling Performance of Lithium-Metal Batteries. *Adv. Mater. Inter.* **2017**, *4*, 1700166. [CrossRef]
15. Rafiz, K.; Murali, D.R.L.; Lin, J.Y. Suppressing lithium dendrite growth on lithium-ion/metal batteries by a tortuously porous γ-alumina separator. *Electrochim. Acta* **2022**, *421*, 140478. [CrossRef]
16. Muchakayala, R.; Yarramsetti, S.; Maram, P.S.; Kalluri, S.; Ran, F.; Sangaraju, S. Modified ceramic coated polyethylene separator—A strategy for using lithium metal as anode with superior electrochemical performance and thermal stability. *J. Energy Storage* **2023**, *68*, 107687. [CrossRef]
17. He, M.; Zhang, X.; Jiang, K.; Wang, J.; Wang, Y. Pure inorganic separator for lithium ion batteries. *ACS Appl. Mater. Interfaces* **2015**, *7*, 738–742. [CrossRef]
18. Mi, W.; Sharma, G.; Dong, X.; Jin, Y.; Lin, Y.S. Electrode-supported thin α-alumina separators for lithium-ion batteries. *J. Power Sources* **2016**, *305*, 209–216. [CrossRef]
19. Parikh, D.; Jafta, C.J.; Thapaliya, B.P.; Sharma, J.; Meyer, H.M.; Silkowski, C.; Li, J. Al2O3/TiO2 coated separators: Roll-to-roll processing and implications for improved battery safety and performance. *J. Power Sources* **2021**, *507*, 230259. [CrossRef]
20. Shi, C.; Dai, J.; Li, C.; Shen, X.; Peng, L.; Zhang, P.; Wu, D.; Sun, D.; Zhao, J. A Modified Ceramic-Coating Separator with High-Temperature Stability for Lithium-Ion Battery. *Polymers* **2017**, *9*, 159. [CrossRef] [PubMed]
21. Yang, C.; Tong, H.; Luo, C.; Yuan, S.; Chen, G.; Yang, Y. Boehmite particle coating modified microporous polyethylene membrane: A promising separator for lithium ion batteries. *J. Power Sources* **2017**, *348*, 80–86. [CrossRef]
22. Zhang, Y.; Wang, Z.; Xiang, H.; Shi, P.; Wang, H. A thin inorganic composite separator for lithium-ion batteries. *J. Membr. Sci.* **2016**, *509*, 19–26. [CrossRef]
23. Schadeck, U.; Kyrgyzbaev, K.; Zettl, H.; Gerdes, T.; Moos, R. Flexible, Heat-Resistant, and Flame-Retardant Glass Fiber Nonwoven/Glass Platelet Composite Separator for Lithium-Ion Batteries. *Energies* **2018**, *11*, 999. [CrossRef]
24. Schadeck, U.; Kyrgyzbaev, K.; Gerdes, T.; Willert-Porada, M.; Moos, R. Porous and non-porous micrometer-sized glass platelets as separators for lithium-ion batteries. *J. Membr. Sci.* **2018**, *550*, 518–525. [CrossRef]
25. Lin, W.; Wang, F.; Wang, H.; Li, H.; Fan, Y.; Chan, D.; Chen, S.; Tang, Y.; Zhang, Y. Thermal-Stable Separators: Design Principles and Strategies Towards Safe Lithium-Ion Battery Operations. *ChemSusChem* **2022**, *15*, e202201464. [CrossRef]
26. Frost, A.R. Rotary atomization in the ligament formation mode. *J. Agric. Eng. Res.* **1981**, *26*, 63–78. [CrossRef]
27. Yuan, C.; Sheldon, B.W.; Xu, J. Heterogeneous Reinforcements to Mitigate Li Penetration through Solid Electrolytes in All-Solid--State Batteries. *Adv. Energy Mater.* **2022**, *12*, 2201804. [CrossRef]
28. Takemura, D.; Aihara, S.; Hamano, K.; Kise, M.; Nishimura, T.; Urushibata, H.; Yoshiyasu, H. A powder particle size effect on ceramic powder based separator for lithium rechargeable battery. *J. Power Sources* **2005**, *146*, 779–783. [CrossRef]
29. Kanhere, N.; Rafiz, K.; Sharma, G.; Sun, Z.; Jin, Y.; Lin, Y.S. Electrode-coated alumina separators for lithium-ion batteries—Effect of particle size and distribution of alumina powders. *Powder Technol.* **2019**, *353*, 230–237. [CrossRef]
30. Hyun, D.-E.; Jung, Y.-J.; Kim, T.-W.; Koo, S.-M.; Park, C.; Kim, H.S.; Kim, S.; Shin, W.H.; Lee, D.-W.; Oh, J.-M. Multi-functional Al2O3-coated separators for high-performance lithium-ion batteries: Critical effects of particle shape. *Ceram. Int.* **2023**, *49*, 30147–30155. [CrossRef]
31. Asghar, M.R.; Anwar, M.T.; Naveed, A.; Zhang, J. A Review on Inorganic Nanoparticles Modified Composite Membranes for Lithium-Ion Batteries: Recent Progress and Prospects. *Membranes* **2019**, *9*, 78. [CrossRef]
32. Liu, H.; Dai, Z.; Xu, J.; Guo, B.; He, X. Effect of silica nanoparticles/poly(vinylidene fluoride-hexafluoropropylene) coated layers on the performance of polypropylene separator for lithium-ion batteries. *J. Energy Chem.* **2014**, *23*, 582–586. [CrossRef]

33. Mun, S.C.; Won, J.H. Estimating the Permeability of the Ceramic Coating on Lithium-Ion Battery Separators via the Ideal Laminate Theory. *Front. Energy Res.* **2022**, *10*, 928179. [CrossRef]
34. Lee, D.-W.; Lee, S.-H.; Kim, Y.-N.; Oh, J.-M. Preparation of a high-purity ultrafine α-Al2O3 powder and characterization of an Al2O3-coated PE separator for lithium-ion batteries. *Powder Technol.* **2017**, *320*, 125–132. [CrossRef]
35. Zhang, P.; Chen, L.; Shi, C.; Yang, P.; Zhao, J. Development and characterization of silica tube-coated separator for lithium ion batteries. *J. Power Sources* **2015**, *284*, 10–15. [CrossRef]
36. Kyrgyzbaev, K.; Rosin, A.; Willert-Porada, M. Influence of temperature on the thickness of ultrathin particulate glass platelets. *Glass Tech. Eur. J. Glass Sci. Technol. A* **2016**, *57*, 95–100. [CrossRef]
37. *ASTM F 1306*; Test Method for Slow Rate Penetration Resistance of Flexible Barrier Films and Laminates. ASTM International: West Conshohocken, PA, USA, 2021.
38. Rank, P.; Hacker, N.; Gerdes, T. Influence of the initial morphology on the dry-milling behavior of glass. *Powder Technol.* **2025**, *467*, 121490. [CrossRef]
39. Garboczi, E.J.; Riding, K.A.; Mirzahosseini, M. Particle shape effects on particle size measurement for crushed waste glass. *Adv. Powder Technol.* **2017**, *28*, 648–657. [CrossRef]
40. Boateng, B.; Zhang, X.; Zhen, C.; Chen, D.; Han, Y.; Feng, C.; Chen, N.; He, W. Recent advances in separator engineering for effective dendrite suppression of Li-metal anodes. *Nano Sel.* **2021**, *2*, 993–1010. [CrossRef]
41. Robbins, J.R.; Ding, J.L.; Gupta, Y.M. Load spreading and penetration resistance of layered structures—A numerical study. *Int. J. Impact Eng.* **2004**, *30*, 593–615. [CrossRef]
42. Gupta, Y.; Ding, J. Impact load spreading in layered materials and structures: Concept and quantitative measure. *Int. J. Impact Eng.* **2002**, *27*, 277–291. [CrossRef]
43. Gao, Y.; Wang, X.; Wang, Y.; Ji, C.; Zhao, C.; Wu, G. Penetration resistance of bioinspired nacre-like SiC ceramic/ASP polyurea structure under projectile impact loading: Experiment and simulation. *Thin-Walled Struct.* **2025**, *208*, 112812. [CrossRef]
44. Liu, Y.; Tzeng, Y.-K.; Lin, D.; Pei, A.; Lu, H.; Melosh, N.A.; Shen, Z.-X.; Chu, S.; Cui, Y. An Ultrastrong Double-Layer Nanodiamond Interface for Stable Lithium Metal Anodes. *Joule* **2018**, *2*, 1595–1609. [CrossRef]
45. Guo, Z.; Liu, Z.; Zhang, Y.; Li, H.; Qi, M.; Zhao, C.; Zhang, X.; Wu, Z.; Yuan, J.; Zhang, N. Ultrastrong bioinspired "brick-and-mortar" artificial SEI for dendrite-free Zn anode. *Matter* **2025**, *2025*, 102269. [CrossRef]
46. Neumann, J.; Hellweg, L.; Bela, M.; Hering, T.; Stan, M.; Winter, M.; Nowak, S.; Börner, M. The role of lithium metal electrode thickness on cell safety. *Cell Rep. Phys. Sci.* **2025**, *6*, 102354. [CrossRef]
47. Koo, D.; Kwon, B.; Lee, J.; Lee, K.T. Asymmetric behaviour of Li/Li symmetric cells for Li metal batteries. *Chem. Commun.* **2019**, *55*, 9637–9640. [CrossRef] [PubMed]
48. Wang, C.; Deng, T.; Fan, X.; Zheng, M.; Yu, R.; Lu, Q.; Duan, H.; Huang, H.; Wang, C.; Sun, X. Identifying soft breakdown in all-solid-state lithium battery. *Joule* **2022**, *6*, 1770–1781. [CrossRef]
49. Chang, Z.; Yang, H.; Pan, A.; He, P.; Zhou, H. An improved 9 micron thick separator for a 350 Wh/kg lithium metal rechargeable pouch cell. *Nat. Commun.* **2022**, *13*, 6788. [CrossRef]
50. Wang, H.; Xu, Z.; An, J.; Noor, S.; Yang, C.; Wang, G. Stable deposition/stripping of lithium metal for long lifespan batteries by shielding electrical double layer interference with a lithiated TiO_2 cap. *J. Alloys Compd.* **2024**, *983*, 173816. [CrossRef]
51. Jana, A.; Ely, D.R.; García, R.E. Dendrite-separator interactions in lithium-based batteries. *J. Power Sources* **2015**, *275*, 912–921. [CrossRef]
52. Cooper, E.R.; Li, M.; Gentle, I.; Xia, Q.; Knibbe, R. A Deeper Understanding of Metal Nucleation and Growth in Rechargeable Metal Batteries Through Theory and Experiment. *Angew. Chem. Int. Ed. Engl.* **2023**, *62*, e202309247. [CrossRef]
53. Li, J.; Mei, B.-A.; Feng, H.; Zuo, Z.; Xiong, R. Lithium dendrite deposition kinetics and its dynamic impact on capacity fading of lithium-ion batteries. *J. Power Sources* **2025**, *654*, 237753. [CrossRef]
54. Li, Z.; Huang, J.; Yann Liaw, B.; Metzler, V.; Zhang, J. A review of lithium deposition in lithium-ion and lithium metal secondary batteries. *J. Power Sources* **2014**, *254*, 168–182. [CrossRef]
55. Permatasari, A.; So, M.; van Nguyen, L.; Yano, T.; Inoue, G. Porosity and tortuosity dynamics and their impact on lithium-ion battery performance with different separator structures. *J. Power Sources* **2025**, *647*, 237278. [CrossRef]
56. Ma, M.; Orhan, A.; Feng, L.; de Beer, M.P.; Troksa, A.L.; Hwee, N.; Heo, T.W.; Biener, J.; Wan, J.; Ye, J. 3D Printed Nanoporous Separators Based on Polymerization-Induced Phase Separation for Fast-Charging, High Cycling Stability Li-Ion Batteries. *ACS Appl. Eng. Mater.* **2024**, *2*, 2245–2254. [CrossRef]
57. Nishi, Y. Lithium ion secondary batteries; past 10 years and the future. *J. Power Sources* **2001**, *100*, 101–106. [CrossRef]
58. Asenbauer, J.; Eisenmann, T.; Kuenzel, M.; Kazzazi, A.; Chen, Z.; Bresser, D. The success story of graphite as a lithium-ion anode material—Fundamentals, remaining challenges, and recent developments including silicon (oxide) composites. *Sustain. Energy Fuels* **2020**, *4*, 5387–5416. [CrossRef]
59. Edge, J.S.; O'Kane, S.; Prosser, R.; Kirkaldy, N.D.; Patel, A.N.; Hales, A.; Ghosh, A.; Ai, W.; Chen, J.; Yang, J.; et al. Lithium ion battery degradation: What you need to know. *Phys. Chem. Chem. Phys.* **2021**, *23*, 8200–8221. [CrossRef]

60. Yang, R.; Yu, G.; Wu, Z.; Lu, T.; Hu, T.; Liu, F.; Zhao, H. Aging of lithium-ion battery separators during battery cycling. *J. Energy Storage* **2023**, *63*, 107107. [CrossRef]
61. Fang, R.; Dong, P.; Ge, H.; Fu, J.; Li, Z.; Zhang, J. Capacity plunge of lithium-ion batteries induced by electrolyte drying-out: Experimental and Modeling Study. *J. Energy Storage* **2021**, *42*, 103013. [CrossRef]